THE ASTROPHYSICAL JOURNAL, 539:L41–L44, 2000 August 10
© 2000. The American Astronomical Society. All rights reserved. Printed in U.S.A.

HIGH-RESOLUTION X-RAY SPECTRA OF CAPELLA: INITIAL RESULTS FROM THE *CHANDRA* HIGH-ENERGY TRANSMISSION GRATING SPECTROMETER

C. R. CANIZARES, D. P. HUENEMOERDER, D. S. DAVIS, D. DEWEY, K. A. FLANAGAN, J. HOUCK, T. H. MARKERT, H. L. MARSHALL, M. L. SCHATTENBURG, N. S. SCHULZ, AND M. WISE
Massachusetts Institute of Technology, Center for Space Research, 70 Vassar Street, Cambridge, MA 02139
AND
J. J. DRAKE AND N. S. BRICKHOUSE
Harvard-Smithsonian Center for Astrophysics, 60 Garden Street, Cambridge, MA 02138
Received 2000 March 10; accepted 2000 June 26; published 2000 August 1

ABSTRACT

High-resolution spectra of the active binary Capella (G8 III + G1 III) covering the energy range of 0.4–8.0 keV (1.5–30 Å) show a large number of emission lines, demonstrating the performance of the High-Energy Transmission Grating Spectrometer. A preliminary application of plasma diagnostics provides information on coronal temperatures and densities. Lines arising from different elements in a range of ionization states indicate that Capella has plasma with a broad range of temperatures, from $\log T = 6.3$ to 7.2, generally consistent with recent results from observations with the *Extreme-Ultraviolet Explorer* and the *Advanced Satellite for Cosmology and Astrophysics*. The electron density is determined from He-like O VII lines, giving the value of $N_e \sim 10^{10}$ cm^{-3} at $T_e \sim 2 \times 10^6$ K; He-like lines formed at higher temperatures give only upper limits to the electron density. The density and emission measure from O VII lines together indicate that the coronal loops are significantly smaller than the stellar radius.

Subject headings: instrumentation: spectrographs — stars: coronae — stars: individual (Capella) — X-rays: general — X-rays: stars

1. INTRODUCTION

The active binary Capella (α Aurigae, HD 34029, HR 1708) was observed with the High-Energy Transmission Grating Spectrometer (HETGS) on the *Chandra X-Ray Observatory*. We present a first analysis of the spectra with the goals of demonstrating the HETGS performance and of applying plasma diagnostics to infer physical parameters of the Capella corona. A complementary analysis of the corona of Capella based on high-resolution spectra obtained using the *Chandra* Low-Energy Transmission Grating Spectrometer (LETGS) has been presented by Brinkman et al. (2000). Further analysis of diagnostic emission lines from these and other *Chandra* grating data of Capella are underway with the goal of obtaining refined temperature-dependent emission measures, abundances, and densities, leading to a self-consistent determination of the coronal structure.

1.1. *The Chandra HETGS*

The High-Energy Transmission Grating assembly (Markert et al. 1994; C. R. Canizares et al. 2000, in preparation) consists of an array of periodic gold microstructures that can be interposed in the converging X-ray beam just behind the *Chandra* High-Resolution Mirror Assembly. When in place, the gratings disperse the X-rays according to wavelength, creating spectra that are recorded at the focal plane by the linear array of CCDs designated ACIS-S. There are two different grating types, designated MEG and HEG, optimized for medium and high energies (partially overlapping in spectral coverage). The HETGS provides spectral resolving power of $\lambda/\Delta\lambda = 100$–1000 for point sources (corresponding to a line FWHM of about 0.02 Å for MEG, and 0.01 Å for HEG) and effective areas of 1–180 cm^2 over the wavelength range of 1.2–30 Å (0.4–10 keV). Multiple overlapping orders are separated using the moderate-energy resolution of the Advanced CCD Imaging Spectrometer (ACIS). The HETGS complements the LETGS, which is optimized for lower energy X-rays.[1]

Preliminary analysis of in-flight calibration data, including those presented here, indicates that the HETGS is performing as predicted prior to the *Chandra* launch. The spectral resolution is as expected, and effective areas are within 10% of the expected values, except from 6 to 12 Å where there are systematic uncertainties of up to 20%. Ongoing calibration efforts will reduce these uncertainties.

1.2. *The Coronal Structure of Capella*

Capella is an active binary system comprised of G1 and G8 giants in a 104 day orbit at a distance of 12.9 pc. The G1 star rotates with an ~8 day period (Hummel et al. 1994). Capella has been studied by many previous X-ray telescopes, including *Einstein* (Holt et al. 1979; Swank et al. 1981; Mewe et al. 1982; Vedder & Canizares 1983; Schmitt et al. 1990), *EXOSAT* (Lemen et al. 1989), *ROSAT* (Dempsey et al. 1993), *BeppoSAX* (Favata et al. 1997), and *ASCA* (Brickhouse et al. 2000). The fundamental parameters of Capella, some activity indicators, and primary references may be found in Strassmeier et al. (1993).

The corona of Capella appears intermediate in temperature, being cooler than those of RS CVn stars such as HR 1099 or II Peg, but significantly hotter than a less active star like Procyon. X-ray observations obtained at low to moderate spectral resolution are generally consistent with emission from an optically thin, collisionally dominated plasma with two temperature components (Swank et al. 1981; Schmitt et al. 1990). Spectra obtained by the *Extreme-Ultraviolet Explorer* (*EUVE*) have provided more discriminating temperature diagnostics, showing plasma over a continuous range of temperatures, with the peak emission measure near $\log T = 6.8$ (Dupree et al.

[1] For detailed descriptions of the instruments, see http://chandra.harvard.edu.

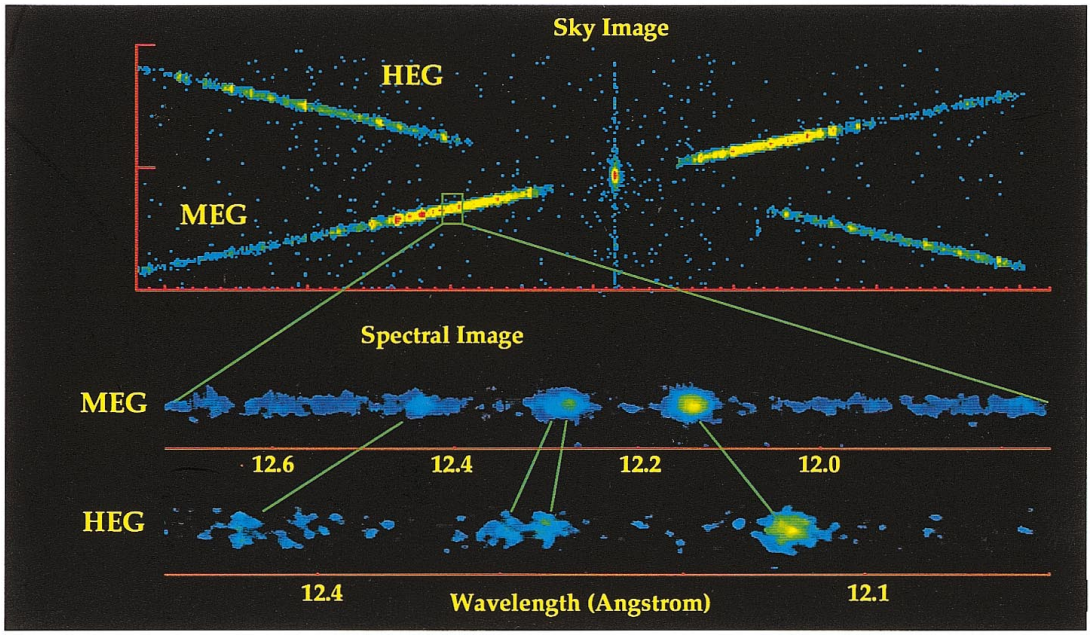

FIG. 1.—*Top*: HETGS spectrum shown as an image in sky coordinates. The zeroth-order image is in the center (the vertical streak is caused by the CCD readout). The orientations of the MEG and HEG gratings are offset, so the spectra form a shallow "x" on the ACIS array. The sky image has been blurred for visual presentation since the distribution is too narrow to see features. A small portion of each spectrum (also smoothed) as labeled is shown at the bottom.

1993; Schrijver et al. 1995; Brickhouse et al. 2000). Simultaneous measurements using *EUVE* and *ASCA* spectra did not require emission from plasma hotter than log $T = 7.3$ (Brickhouse et al. 2000). *EUVE* observations show variability by factors of 3–4 in lines formed above log $T \sim 7.0$ (Brickhouse et al. 2000; A. K. Dupree, N. S. Brickhouse, & J. Sanz-Forcada 2000, in preparation).

Dupree et al. (1993) have estimated plasma electron densities in the range from 4×10^{11} to 10^{13} cm^{-3} from lines of Fe XXI formed near $10^{6.8}$ K, implying that the scale of the emitting volume is $\sim 10^{-3}\ R_*$, although Griffiths & Jordan (1998) question the reliability of this diagnostic. Brickhouse et al. (2000) use EUV lines of Fe XVIII to constrain the optical depth in the strong X-ray emission line Fe XVII λ15.014 to $\tau < 3.6$.

From high-resolution UV spectra from the *Hubble Space Telescope*, Linsky et al. (1998) concluded that both stars have comparable coronal emission, based on measurements of the Fe XVII (1354 Å) coronal forbidden line, and that the plasma is magnetically confined. Thus, the "corona" of Capella is actually a composite of two "coronae."

2. OBSERVATIONS AND DATA PROCESSING

We combined data from three HETGS observations (from 1999 August 28 and September 24 and 25) for a total exposure of 89 ks. Data were processed with the standard *Chandra* X-ray Center software (versions from July 29 [R4CU3UPD2] and December 13 [CIAO 1.1]). The image of the dispersed spectrum is shown in Figure 1. Each photon is assigned a dispersion angle θ relative to the undiffracted zero-order image. The angle is related to the order m and wavelength λ through the grating mean period P by the grating equation $m\lambda = P \sin\theta$. The spectral order is determined using the ACIS-S CCD pulse height for each photon event (with wide latitude to avoid sensitivity to variations in CCD gain or pulse-height resolution). The positive and negative first orders were summed separately for HEG and MEG for all observations and divided by the effective areas to provide flux-calibrated spectra (Fig. 2). Selected spectral features are listed in Table 1. We note that the Fe XVII λ15.01 line strength is, within the uncertainties, identical to that observed in 1979 by Vedder & Canizares (1983) with the *Einstein* crystal spectrometer, while the O VIII Lyα line is roughly half the previous value.

3. CORONAL DIAGNOSTICS

3.1. *Emission Measure Distribution*

Some properties of the coronal temperature structure can be deduced from a preliminary analysis of the spectrum. The data warrant a full analysis of the volume emission measure distribution with temperature VEM(T) [VEM(T) $\propto N_e^2 V$, in which N_e is the electron density of plasma at temperature T that occupies the volume V], which will be the subject of a future paper.

As Table 1 illustrates, the spectrum contains lines from different elements in a range of ionization states, demonstrating that the emitting plasma has a broad range of temperature. Further evidence of multitemperature emission comes from two line ratios. First, ratios of H-like to He-like resonance lines of O VIII/O VII, Mg XII/Mg XI, and Si XIV/Si XIII indicate ionization ratios corresponding to log $T = 6.55$–6.60, 6.75–6.85, and 6.95–7.00, respectively. Second, the He-like ions provide temperature-sensitive ratios involving the resonance (r), forbidden (f), and intersystem (i) lines (Gabriel & Jordan 1969; Gabriel 1972; Pradhan & Shull 1981; R. Smith, N. Brickhouse, J. Raymond, & D. Liedahl 1998[2]). For the observed O VII, Mg XI, and Si XIII lines, the ratio $(i + f)/r$ corresponds to temperatures log $T = 6.2$–6.4, 6.9–7.1, and 6.85–6.95, respectively, using the theoretical models of R. Smith, N. Brick-

[2] Available at http://xmm.vilspa.esa.es/news/ws1/ws1_papers.html.

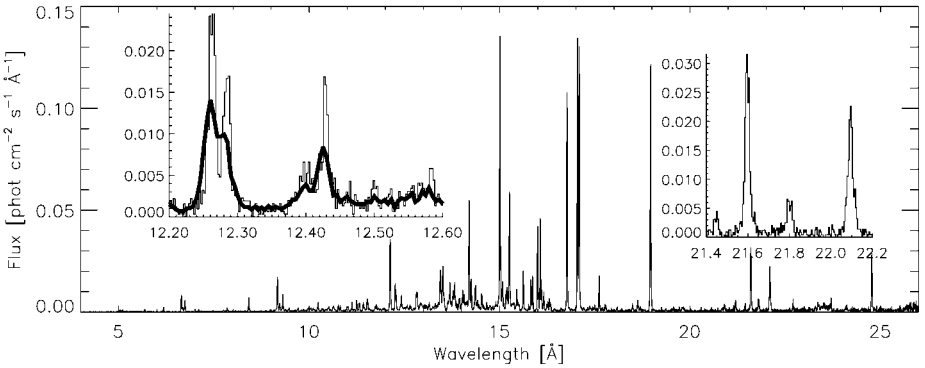

FIG. 2.—Merged MEG spectrum of order ±1 together with two insets. *Left*: A region that compares the HEG (*thin line*) with the MEG. *Right*: O VII He-like triplet.

house, J. Raymond, & D. Liedahl (1998; in the low-density limit). In both cases, the ratios indicate that the corona has a broad range of temperature.

An approximate upper envelope to the true VEM distribution is given by the family of curves formed by plotting the ratio of line strength to corresponding emissivity for a collection of lines. For a given element, its abundance affects only the overall normalization of the envelope of all lines from that element. For this initial analysis, we assumed solar abundances (Anders & Grevesse 1989); this analysis is consistent with previous analyses except possibly for Ne (Brickhouse et al. 2000).

The VEM envelope of Figure 3 indicates that plasma must be present over nearly a decade in temperature. The absence of lines from He-like and H-like ions of Fe provides an upper limit to the VEM above $\log T = 7.2$. Although the envelope does not trace closely the peaked distribution derived from EUV lines, such a distribution is not excluded.

TABLE 1
SELECTED EMISSION LINES FROM MEG

Line	λ[a] (Å)	Flux[b] (photons cm^{-2} s^{-1})	C[c]	T_m[d] (K)
Fe XXV	1.85	<4	<7	7.8
S XV	5.040	33	110	7.2
S XV	5.060	16	55	7.2
S XV	5.100	26	85	7.2
Si XIII	5.680	25	93	7.0
Si XIV	6.180	48	472	7.2
Si XIII	6.650	182	1228	7.0
Si XIII	6.690	47	374	7.0
Si XIII	6.740	121	834	7.0
Al XII	7.750	16	204	6.9
Mg XII	8.419	152	1947	7.0
Mg XI	9.170	348	2818	6.8
Mg XI	9.230	63	618	6.8
Mg XI	9.310	190	1425	6.8
Ne X	10.240	92	740	6.8
Ni XXII	10.791	62	426	7.0
Ne X[e]	12.132	929	4171	6.8
Fe XVII[e]	12.134	...	...	6.8
Fe XIX[e]	13.515	530	1587	6.9
Fe XIX[e]	13.524	...	...	6.9
Fe XVII	15.013	3043	7476	6.7
Fe XVII	15.272	1119	2919	6.7
Fe XVIII	15.641	410	938	6.8
O VIII	16.003	898	1885	6.5
Fe XVII	16.796	2004	3669	6.7
Fe XVII	17.071	2641	4554	6.7
Fe XVII	17.119	2443	4191	6.7
O VIII	18.967	2634	2810	6.5
O VII	21.600	967	396	6.3
O VII	21.800	255	102	6.3
O VII	22.100	736	249	6.3
N VII	24.779	549	327	6.3

[a] Theoretical wavelengths of identification.
[b] The observed flux is 10^{-6} times the tabulated flux. The systematic uncertainty is less than 10%, except in the range from 6 to 12 Å where it is up to 20%.
[c] Integrated line counts in 89 ks.
[d] The log temperature of maximum emissivity.
[e] Blend; entry for sum of two components.

3.2. *Density Diagnostics*

The He-like f/i ratio is primarily sensitive to density. Using the theoretical line ratios of R. Smith, N. Brickhouse, J. Raymond, & D. Liedahl (1998; see footnote 2), our measured O VII ratio of 2.9 ± 0.4 implies an electron density within the range of $(0.8–2) \times 10^{10}$ cm^{-3}. Similarly, the Mg XI and Si XIII ratios

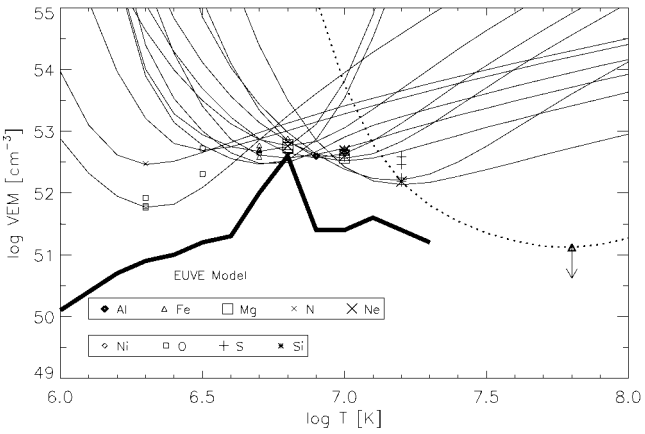

FIG. 3.—VEM distribution based on analysis of our HETGS spectra and from earlier work. The symbols mark the VEM that would correspond to the case in which all the observed emission for the line originates in an isothermal plasma with a temperature corresponding to the peak in the emissivity for that line. These points are shown for selected lines from Table 1 spanning a range in formation temperature. For a few of these, the curved lines are the loci corresponding to the VEM required to produce the observed flux from an isothermal plasma as a function of plasma temperature. The dotted line is an upper limit based on the observed counts in the vicinity of the Fe XXV resonance line (1.85 Å). The thick solid line is the emission measure distribution derived from ultraviolet and extreme-ultraviolet emission lines by Brickhouse (1996) plotted for $d \log T = 0.1$.

of 3.0 ± 0.3 and 2.6 ± 0.2 give upper limits near 7×10^{11} and 1×10^{12} cm^{-3}, respectively. We note that our ratio *f*/*i* for O VII is somewhat lower than that obtained by Brinkman et al. (2000) from LETGS spectra. The HETGS and LETGS observations were not simultaneous; however, based on evidence from prior *EUVE* observations (A. K. Dupree, N. S. Brickhouse, & J. Sanz-Forcada 2000, in preparation), we would be surprised if this difference represented actual changes in the mean coronal plasma density. Instead, we suggest that this results from different treatments of the continuum plus background, which particularly affects the strength of the intercombination line.

4. DISCUSSION

These X-ray data confirm that Capella's corona contains plasma at multiple temperatures in the accessible range from $\log T \sim 6.3$ to 7.2, and we set stringent constraints on the amount of plasma hotter than $\log T = 7.2$ at the time of this observation. These properties are generally consistent with the results found with *EUVE* and *ASCA* (Brickhouse et al. 2000), and the line strengths are close those seen 20 years earlier by Vedder & Canizares (1983).

The preliminary results presented here have implications for the structure of Capella's corona: they suggest that the characteristic dimensions of the coronal loops at $T \sim 2 \times 10^6$ K are small compared with the stellar radius R_*. For simple semicircular loops of constant circular cross section of radius r, we use the measured density and VEM for oxygen to estimate loop heights $\leq 0.02\ R_* \alpha_{0.1}^{-2/3} N_{100}^{-1/3}$, where $\alpha_{0.1}$ is the ratio of r to loop length in units of 0.1 and N_{100} is 1/100 the number of loops. The detailed loop modeling of van den Oord et al. (1997) also required compact structures, although variable cross section loops were needed to increase the proportion of hot to cool plasma.

Work at MIT was supported by NASA through the HETG contract NAS8-38249 and through Smithsonian Astrophysical Observatory (SAO) contract SVI-61010 for the *Chandra* X-ray Center (CXC). J. J. D. and N. S. B. were supported by NASA contract NAS8-39083 to SAO for the CXC. We thank all our colleagues who helped develop the HETGS and all members of the *Chandra* team.

REFERENCES

Anders, E., & Grevesse, N. 1989, Geochim. Cosmochim. Acta, 53, 197
Brickhouse, N. S. 1996, in IAU Colloq. 152, Astrophysics in the Extreme Ultraviolet, ed. S. C. Bowyer & R. F. Malina (Dordrecht: Kluwer), 105
Brickhouse, N. S., Dupree, A. K., Edgar, R. J., Liedahl, D. A., Drake, S. A., White, N. E., & Singh, K. P. 2000, ApJ, 530, 387
Brinkman, A.C., et al. 2000, ApJ, submitted
Dempsey, R. C., Linsky, J. L., Schmitt, J. H. M. M., & Fleming, T. A. 1993, ApJ, 413, 333
Dupree, A. K., Brickhouse, N. S., Doschek, G. A., Green, J. C., & Raymond, J. C. 1993, ApJ, 418, L41
Favata, F., Mewe, R., Brickhouse, N. S., Pallavicini, R., Micela, G., & Dupree, A. K. 1997, A&A, 324, L37
Gabriel, A. H. 1972, MNRAS, 160, 99
Gabriel, A. H., & Jordan, C. 1969, MNRAS, 145, 241
Griffiths, N. W., & Jordan, C. 1998, ApJ, 497, 883
Holt, S. S., White, N. E., Becker, R. H., Boldt, E. A., Mushotzky, R. F., Serlemitsos, P. J., & Smith, B. W. 1979, ApJ, 234, L65
Hummel, C. A., Armstrong, J. T., Quirrenbach, A., Buscher, D. F., Mozurkewich, D., & Elias, N. M., II. 1994, AJ, 107, 1859
Lemen, J. R., Mewe, R., Schrijver, C. J., & Fludra, A. 1989, ApJ, 341, 474
Linsky, J. L., Wood, B. E., Brown, A., & Osten, R. A. 1998, ApJ, 492, 767
Markert, T. H., Canizares, C. R., Dewey, D., McGuirk, M., Pak, C. S., & Schattenburg, M. L. 1994, Proc. SPIE, 2280, 168
Mewe, R., et al. 1982, ApJ, 260, 233
Pradhan, A. K., & Shull, J. M. 1981, ApJ, 249, 821
Schmitt, J. H. M. M., Collura, A., Sciortino, S., Vaiana, G. S., Harnden, F. R., Jr., & Rosner, R. 1990, ApJ, 365, 704
Schrijver, C. J., Mewe, R., van den Oord, G. H. J., & Kaastra, J. S. 1995, A&A, 302, 438
Strassmeier, K. G., Hall, D. S., Fekel, F. C., & Scheck, M. 1993, A&AS, 100, 173
Swank, J. H., Holt, S. S., White, N. E., & Becker, R. H. 1981, ApJ, 246, 208
van den Oord, G. H. J., Schrijver, C. J., Camphens, M., Mewe, R., & Kaastra, J. S. 1997, A&A, 326, 1090
Vedder, P. W., & Canizares, C. R. 1983, ApJ, 270, 666